ADVANCED ENERGY MATERIALS
www.advenergymat.de

Fluid Oscillation-Driven Bi-Directional Air Turbine Triboelectric Nanogenerator for Ocean Wave Energy Harvesting

Shaohui Yang, Chengzhuo Zhang, Zhichang Du, Yongqiang Tu, Xianggang Dai, Yan Huang, Jianyu Fan, Zhanyong Hong, Tao Jiang,* and Zhong Lin Wang**

Ocean wave energy is one of the important renewable energy sources. However, random, low-frequency, and micro-amplitude characteristics of ocean waves make it difficult for traditional electromagnetic generators to collect wave energy efficiently. The emergence of triboelectric nanogenerator (TENG) provides an extremely effective technical means for the collection of low-frequency and micro-amplitude wave energy. In this work, a non-contact turntable-structured oscillating water column TENG (OWC-TENG) is designed by combining an OWC wave energy conversion mechanism with a TENG for the first time. The OWC is optimized through simulation experiments according to the principles of ship hydrostatics and wave theory. The output performances of the OWC-TENGs with different structural parameters under different water wave excitation conditions are then tested. The TENG delivers a maximum output current of 55.45 μA and an output power of 5.28 mW, which corresponds to a power density of 114.8 W m^{-3}, enabling a stable power supply for small sensors at sea. This work provides a new solution to the efficient collection of low-frequency micro-amplitude ocean wave energy for powering various offshore equipments, presenting broad application prospects in ocean blue energy development and offshore Internet of Things.

1. Introduction

In recent decades, our daily lives have been largely dependent on the use of fossil fuels for energy, but it poses a threat to the environment. The development of renewable energy sources is therefore crucial.[1–3] Ocean wave energy is one of the most promising energy sources, which is widely distributed, abundant, and unaffected by seasonal, diurnal, and weather variations.[4–7] Conventional wave energy converters are based on electromagnetic generators. Due to its complex structure and large size, the electromagnetic generator still suffers from high cost, low reliability, and low efficiency. To solve this barrier, oscillating conversion devices are used, having unique advantages, one of which is the realization of wave energy conversion in low-frequency waves (≈0.1 Hz). Especially, in 2012, Wang's group proposed the triboelectric nanogenerator (TENG), which is a powerful technology to convert mechanical energy into electrical energy by coupling triboelectrification and electrostatic induction.[8–10] Since its invention, a variety of TENGs with different structures and functions have been developed, gradually innovating mankind's concept of energy harvesting.[11–14]

Although many TENGs exist for ocean wave energy harvesting, the harsh nature of the marine environment, such as seawater corrosion and wave impact, makes the TENGs

S. Yang, C. Zhang, Z. Du, Y. Tu, Y. Huang, J. Fan
College of Marine Equipment and Mechanical Engineering
Jimei University
Xiamen 361021, P. R. China

C. Zhang, X. Dai, Z. Hong, T. Jiang, Z. L. Wang
CAS Center for Excellence in Nanoscience
Beijing Key Laboratory of Micro-Nano Energy and Sensor
Beijing Institute of Nanoenergy and Nanosystems
Chinese Academy of Sciences
Beijing 101400, P. R. China
E-mail: hongzhanyong@binn.cas.cn; jiangtao@binn.cas.cn; zhong.wang@mse.gatech.edu

X. Dai, Z. Hong, T. Jiang
School of Nanoscience and Engineering
University of Chinese Academy of Sciences
Beijing 100049, P. R. China

Z. Hong, T. Jiang, Z. L. Wang
Guangzhou Institute of Blue Energy
Knowledge City
Huangpu District, Guangzhou 510555, P. R. China

Z. L. Wang
Yonsei Frontier Lab
Yonsei University
Seoul 03722, Republic of Korea

The ORCID identification number(s) for the author(s) of this article can be found under https://doi.org/10.1002/aenm.202304184

DOI: 10.1002/aenm.202304184

susceptible to damage. Second, there are difficulties in collecting and converting wave energy due to the irregularity and instability of waves. Variations in the intensity, direction, and period of waves may lead to instability in power generation capacity, which in turn leads to a relatively low utilization of waves by the TENGs as well.[15–18] Therefore, it is urgent to design and optimize the TENGs that can adapt to various environmental conditions. For instance, Ventura et al. developed a buoy-structured TENG device that can be optimized by modulating the moving body velocity by the sea state.[19] Also developing more efficient wave energy harvesting and conversion technologies is needed to improve the utilization of waves by the TENGs.[20–23] The TENGs could be easily packaged and integrated into an oscillating water column (OWC) due to their low manufacturing cost and lightweight.

An oscillating water column TENG (OWC-TENG) utilizes air fluid as an intermediate medium, which is converted into mechanical shaft power rotation using a turbine, and further converted into electrical energy without coming into contact with corrosive seawater. All moving components are mounted above the water surface, largely extending the life of the device. The OWC technology enables the renewable utilization of natural resources, such as ocean waves, reducing dependence on traditional energy sources with low impacts on the marine environments. It can generate a larger propulsive force in a smaller range of wave frequencies, having a higher wave energy utilization rate and adaptability, which can be applied to different marine environmental conditions, even very harsh marine ones. The OWC-TENG can also be used in terrestrial water bodies or rivers for wide applications, and generate electrical power stably in irregularly fluctuating marine environments, demonstrating excellent sustainability and stability. The OWC-TENG adopts a non-contact turntable mode in its structure, which reduces the resistance between two kinds of triboelectric materials and largely improves the durability and mechanical rotation speed. It also has the advantages of high contact-friction output, low wear, low mechanical shock, and high-frequency electrical output. In this work, the output performances of the OWC-TENGs with different structural parameters are investigated. The effects of water wave conditions, such as water wave frequencies and amplitudes, on the OWC-TENG outputs are studied. The anemometer and wireless temperature sensor are then successfully powered to work stably by the water wave triggering. Compared to conventional OWC electromagnetic generators, the OWC-TENG is small, lightweight, low-cost, and stably scalable.[24–26]

2. Results and Discussion

2.1. Structural Design and Work Principles

The OWC-TENG consists of two components, which are the OWC wave energy converter and the bidirectional air turbine TENG. Its working principle and 3D structure are shown in **Figure 1**. The flow of seawater triggers pressure changes inside the chamber when waves act on the OWC-TENG. When the waves push the OWC-TENG up, the pressure in the air chamber inside the main float increases, while when the waves make the OWC-TENG drop, the pressure inside the air chamber decreases. This is shown in Figure 1a. The fluid passes through the guide vanes of the bidirectional air turbine and gets inside the OWC by the fluid movement generated by wave vibrations (caused by the pressure difference between inside and outside). The kinetic energy is transferred to the rotor and further converted into electrical energy by using TENG, resulting in energy conversion as shown in Figure 1b. The 3D structure of TENG and the cross-section of the carousel-type rotating structure is illustrated in Figure 1c,d. The innovation of this design is the combination of the OWC technology with a TENG for the first time, which can achieve efficient harvesting and utilization of water wave energy. The TENG is small and easy to integrate into the OWC system, providing a new and efficient energy harvesting solution. The innovative combination of power take-off technology and power generating technology brings new opportunities in the field of renewable wave energy development.

The bidirectional air turbine TENG consists of two main components: the cylindrical housing and the air turbine. The primary function of the cylindrical housing is to direct and control the flow direction of the fluid, by guiding the fluid to the guide vanes. The housing is one of the most important supporting components of the turbine structure and plays a key role in fixing, connecting, and maintaining the mechanical stability of the turbine. The turbine model was inspired by the relevant research of Setoguchi's team and has been modified accordingly to integrate with TENG.[27,28] To further reduce friction between the rotor and stator and to increase the output capacity, planar thrust ball bearings are used between adjacent turntables.

Considering the uniqueness of the turbine structure, a layered friction start is used. The rotor has four fan-shaped fluorinated ethylene propylene (FEP) layers adhered to one side of the rotor. One side of the stator is coated with copper grid electrodes with four pairs of complementary electrodes. In addition, a nylon film is adhered to the copper electrode discs, and four thin slots are cut to accommodate four rabbit hair brushes of the same size. This design aims to generate triboelectric charges between the stator end and the adjacent rotor end. This non-contact structure effectively decreases the inherent frictional damping of the device without reducing the charge output, significantly reduces the surface wear of the device, and enhances the robustness and durability of the device. The number of integrated sub-units is easily expandable, and one rotor disk intercalated with two stator disks is typically adopted in this work to form two TENG sub-units in total, as schematically shown in Figure 1e. Stages I–IV in Figure 1f indicate the process of the charge flow across the external circuit. The rotor disk is first charged by rotary triboelectrification with the nylon. Then, the relative motion between the rotor disk and the stator disk drives free electrons to move between the two electrodes on the stator due to electrostatic induction, generating alternating current.

In this study, theoretical calculations and simulations are carried out for the design of the OWC device. Assuming that the fluid is a spinless, incompressible ideal fluid, the OWC is simplified to an equal-diameter cylinder. Considering the small amplitude of the motion of the floating body, the study can be carried out using a linear theory by neglecting the mooring

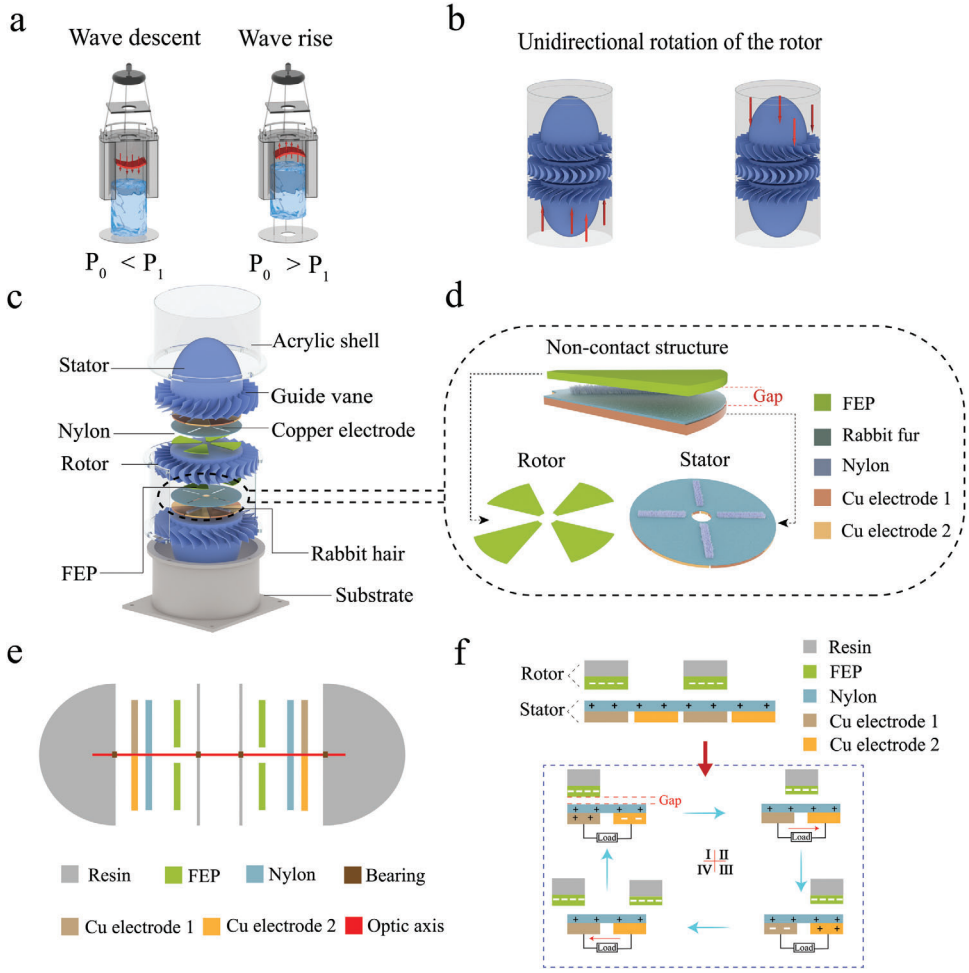

Figure 1. Operation principle and 3D structure of the OWC-TENG. a) Schematic diagram of the OWC-TENG in water waves. b) Working process of bidirectional air turbine. c) Schematic diagram of the 3D structure of the OWC-TENG. d) Schematic diagrams of the rotor and stator discs. e) Cross-section of the OWC-TENG power generation. f) Operation principle of the TENG subunit.

forces on the device and using slack mooring. Only the pendant motion has a positive effect on the power generation, while the other degrees of freedom have a lesser effect on the energy conversion performance. To simplify the computational effort, the focus is on the vertical motion of the OWC. A mathematical model of the motion of the OWC wave energy device is developed concerning the principles of hydrostatics of ships and wave theory.[29]

Under linear wave loading, the dynamic equation of the device can be expressed as:

$$[M + \Delta M]\ddot{\xi}_i + \left[B_{\text{rad}} + B_{\text{vis}}\right]\dot{\xi}_i + \left[K_{\text{sw}} + K_{\text{m}}\right]\xi_i = \left[F_i\right] \tag{1}$$

where ξ_i is the amplitude of motion of the floating body in six degrees of freedom; M is the device mass matrix; ΔM is the additional mass matrix of the device; B_{rad} is the radiative damping matrix; B_{vis} is the viscous damping matrix; K_{sw} is the hydrostatic stiffness; K_{m} is the mooring stiffness; and F_i is wave excitation force on the device.

Expression for the intrinsic period of the device's degrees of freedom of motion is given by

$$T_i = 2\pi\sqrt{\frac{M_{ii} + \Delta M_{ii}}{K_{ii,sw} + K_{ii,m}}} \tag{2}$$

The device mass matrix is

$$M_{ij} = \begin{bmatrix} M & 0 & 0 & 0 & M_{z_G} & -M_{y_G} \\ 0 & M & 0 & -M_{z_G} & 0 & M_{x_G} \\ 0 & 0 & M & M_{y_G} & -M_{x_G} & 0 \\ 0 & -M_{z_G} & M_{y_G} & I_{xx} & I_{xy} & I_{xz} \\ M_{z_G} & 0 & -M_{x_G} & I_{yx} & I_{yy} & I_{yz} \\ -M_{y_G} & M_{x_G} & 0 & I_{zx} & I_{zy} & I_{zz} \end{bmatrix} \tag{3}$$

where M is the mass of the device; (x_G, y_G, z_G) is the position of the device's center of gravity; and I_{ii} is the inertial mass.

The stiffness matrix is given by

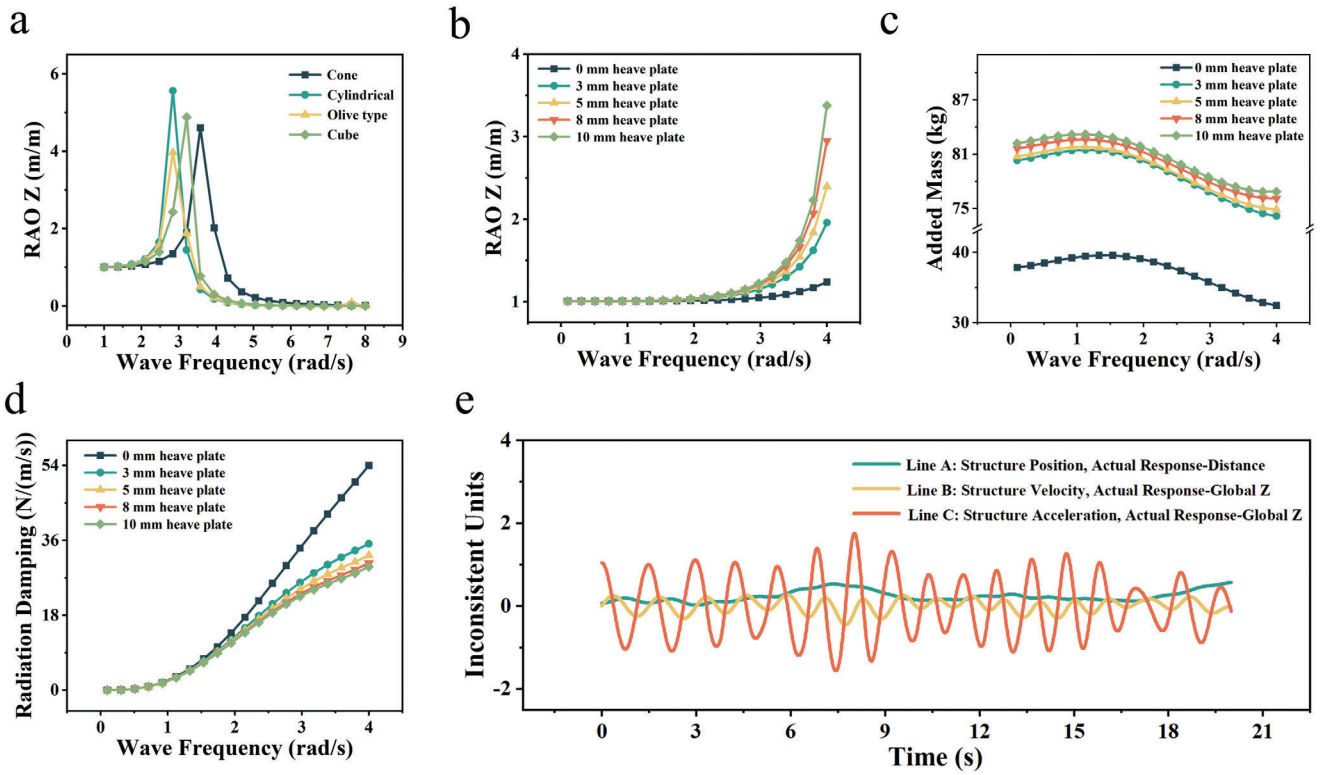

Figure 2. Hydrodynamic force versus wave frequency for OWC wave energy converter. a) RAO Z-diagrams for wave energy converters of different shapes. b) RAO Z plot for the heave plate with different thicknesses. c) Plot of additional mass of heave plate of different thicknesses. d) Plot of damping coefficients for different heave plate thicknesses. e) Motion response plots of the OWC wave energy converter in a wave-making tank.

$$K_{ij,sw} = \begin{bmatrix} 0 & 0 & 0 & 0 & 0 & 0 \\ 0 & 0 & 0 & 0 & 0 & 0 \\ 0 & 0 & \rho g S & \rho g S_2 & -\rho g S_1 & 0 \\ 0 & 0 & \rho g S_2 & \rho g\left(S_{22} + V_{ZB}\right) - Mgz_G & -\rho g S_{12} & -\rho g V_{XB} + Mgx_G \\ 0 & 0 & \rho g S_1 & -\rho g S_{12} & \rho g\left(S_{11} + V_{ZB}\right) - Mgz_G & -\rho g V_{YB} + Mgy_G \\ 0 & 0 & 0 & 0 & 0 & 0 \end{bmatrix} \quad (4)$$

where S is the waterline surface area; S_i is the waterline area first order moments; and S_{ij} is the waterline area second order moments.

Each order moment of the above equation is defined as follows

$$S_i = \iint_S x_i \mathrm{d}s \ , \ S_{ij} = \iint_S x_i x_j ds \quad (5)$$

$$V_i = \iiint_V x_i dv \ , \ V_{ij} = \iiint_V x_i x_j dv \quad (6)$$

The object of this study is a structure that has symmetry and can be reduced to a cylinder. For an OWC wave energy device, only the pendular motion is beneficial for its energy conversion, and the effect of other degrees of freedom on the energy conversion is neglected. We can therefore simplify Equation (1)

$$[M + \Delta M]\ddot{z} + \left[B_{rad} + B_{vis}\right]\dot{z} + \left[K_{sw} + K_m\right] z = \left[F_z\right] \quad (7)$$

where ΔM is the added mass of the device pendulum oscillations and B_{vis} is the device drooping oscillation damping coefficient.

Equation (7) is the motion equation of the center tube wave energy generating device drooping oscillations under the action of linear waves.

The OWC wave energy converter consists of a main float, an internal air chamber, and a heave plate, and the overall shape consists of a cylinder with a height of 1 m and a diameter of 0.6 m. More details can be found in Figure S1, Supporting Information. One of the functions of the main float is to provide buoyancy

and includes a large chamber for receiving incident waves and generating oscillations in the internal water column. The bottom and side walls are partially submerged by seawater, and the volume of stagnant air above the surface is alternately compressed and decompressed. The bidirectional air turbine is driven to rotate as the airflow reciprocates exhalation and inhalation through ducts above the chamber. Therefore, the volume of the internal air chamber is increased as much as possible to achieve higher airflow velocity while ensuring the buoyancy of the overall device.

In this study, the feasibility of the desired floating body structure was verified through the exploration of simulation experiments, the results of which can be seen in **Figure 2**. First, the vertical motion of four common shapes of OWC wave energy converters was systematically investigated (Figure 2a). The RAO Z (Z-direction response amplitude operator) values of all four shapes of OWCs tend to increase and then decrease as the water wave frequency increases, but the cylindrical OWC has the highest RAO Z value in the wave frequency range from 1 to 8 rad s^{-1}. Higher values of RAO Z indicate that the float produces a greater motion response when subjected to the same wave excitation. The implication is that the cylindrical OWC may be more susceptible to wave action and produce greater motion response. That may be because the cylindrical shape could produce higher flow field non-uniformity and larger motion inertia of the system caused by the free liquid level. Furthermore, the shape can adjust its position on the submissive mooring according to the different directions of waves, thus effectively absorbing wave energy from any direction.

In addition, a circular heave plate was used to avoid instability and structural damage to the main float. At the same time, it reduces energy loss and environmental fluctuations and increases the additional mass of the device. The motion response simulation of an austenitic ship was analyzed for different thicknesses of heave plates (Figure 2b). The results show that there is a positive correlation between the increase in the heave plate thickness and the increase in the relative motion amplitude. The relative motion amplitude increases as the thickness of the heave plate increases. To determine the heave plate thickness, further simulation analysis was carried out, and the results are shown in Figure 2c,d. Without a heave plate, the added mass of the OWC is 39.56 kg and the pendant damping is up to 53.99 N m^{-1} s. The added mass of the float is the mass of surrounding water driven by the float as it moves through the water, which is a parameter that expresses the reaction force of fluid and is used to describe the phenomenon of increased inertial forces as an object moves through a fluid. With the increase in the thickness of the heave plate, the added mass of the OWC gradually increases to 81.82 kg, but the pendant damping gradually decreases to 29.65 N m^{-1} s. Regarding the effect of the water wave frequency, the added masses for different thicknesses of heave plates show an increasing and then decreasing trend with the increase of water wave frequency. Taking the above conditions into account, in order to make the floats better convert wave energy into mechanical energy and collect the energy efficiently, we finally chose the thickness of the heavy plate as 5 mm.

Through calculations, the draft depth and mass under the 5 mm-thick pendant oscillating plate were obtained to be 0.71 m and 49.95 kg, respectively, and the results can be viewed in Figure S2, Supporting Information. In order to maximize the motion state of the float in the water, so as to better realize the conversion of wave energy to fluid mechanical energy, we simulated the motion state of the float using the experimental wave pool as the boundary condition, as shown in Figure 2e. After the simulation, the maximum acceleration of the float in the *z*-axis direction can reach 1.76 m s^{-2}, and the maximum displacement distance and instantaneous velocity are 0.58 m and 0.31 m s^{-1}, respectively, under the low-frequency and low-amplitude conditions. The device meets our experimental requirement of efficiently converting wave energy under the excitation of low-frequency and low-amplitude water waves, and the offset angles of the device in the *x*-axis and *y*-axis are no more than 50°, while the simulations of the other degrees of freedom are shown in Figure S3, Supporting Information. Subsequently, the motion state of OWC-TENG in water waves can be seen in Video S1, Supporting Information, which proves that the simulation study of the OWC device is in full agreement with the experimental results.

2.2. Electrical Properties of OWC-TENG

As shown in Figure S4, Supporting Information, the ability of OWC to convert wave energy into fluid mechanical energy varies under different excitation conditions, so it is crucial to determine the best working conditions of OWC for energy conversion. We simulate the wave conditions in the ocean with a wave tank, and the results show that the output signals of the OWC are the largest and stablest when the water wave frequency is 0.83 Hz and the wave height is 0.25 m, showing the strongest energy conversion capability.

Different gaps between the stator and rotor of the OWC-TENG affect the output performances of the device, and the effective contact area under different gaps has a direct influence on the charge transfer. Under the water wave excitations at 0.83 Hz and 0.25 m, we tested the output performances of the OWC-TENGs with different rotor-stator gaps, as shown in **Figure 3**a,b. The results show that the output performance of the OWC-TENG tends to increase and then decrease as the gap increases. When the gap is around 0.8 mm, due to machining and 3D printing errors, there is partial contact between the rotor and stator, which increases the damping and reduces the rotational speed, and thereby the outputs are reduced. The rotation cannot be sustained under low frequency and low amplitude water excitation. The outputs are the highest at a gap of 1 mm with an output current of 23.65 μA, output voltage of 266.92 V, transferred charge of 141.42 nC, and rotor speed of 819 rpm. Since we use a Cu electrode plate with eight grids, one cycle is taken from two adjacent wave crests of the output waveform, and four cycles represent one turn of the rotor. The output data of 10 s are extracted to calculate the average rotor speed and finally get the rotor speed per minute. It is worth noting that when the gap between the stator and rotor is too small, the startup and rotation of the rotor will be affected by motion and rotational friction, as well as rabbit fur friction damping, which prevents it from starting effectively and outputting signals outward. As the gap increases, the rotor speed gradually increases. The rabbit fur and FEP cannot make effective contact, and the output performance of the OWC-TENG decreases significantly.

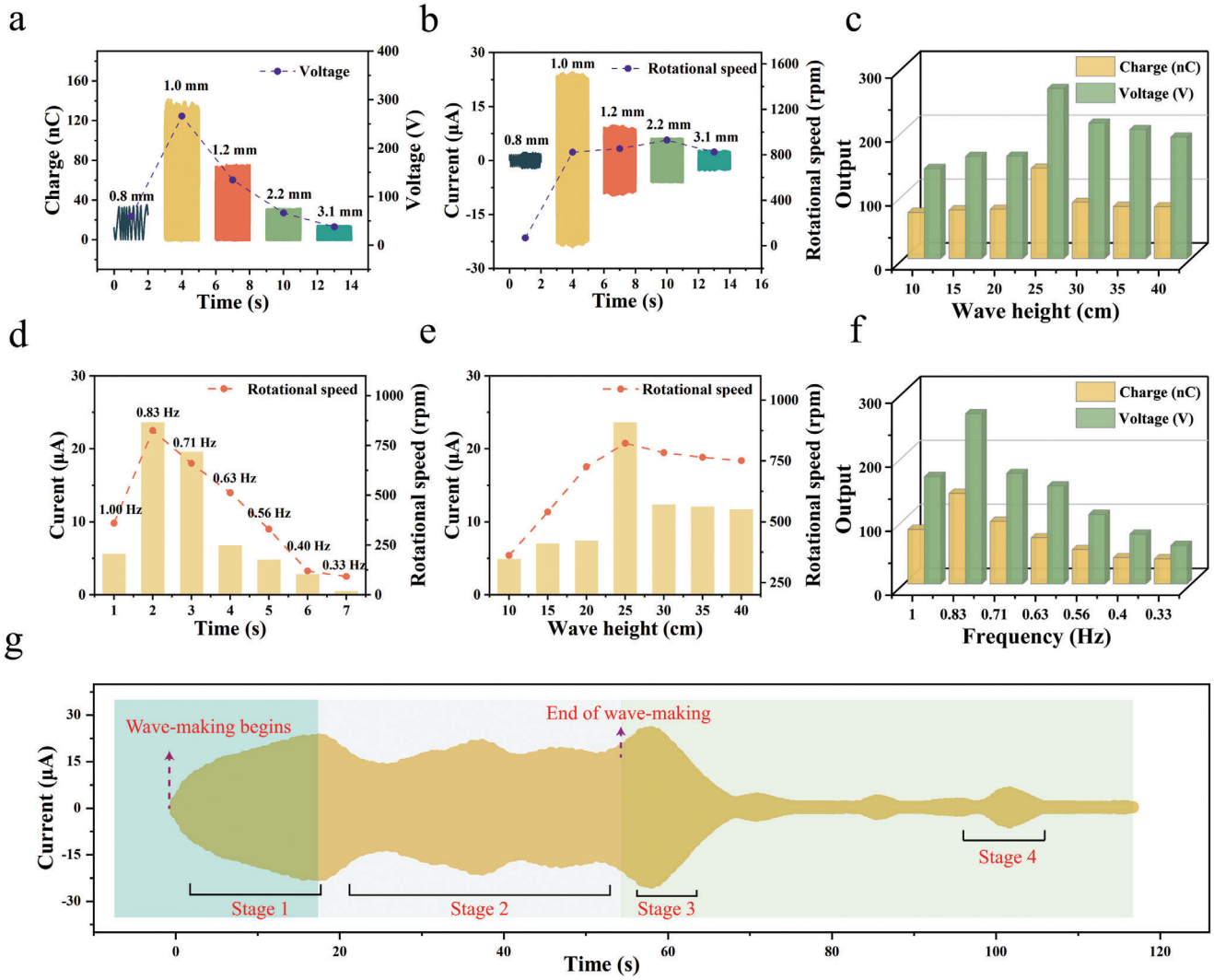

Figure 3. Output performance of OWC-TENG underwater wave triggering. a,b) Output performance of OWC-TENG under different gaps. c–f) Effect of different water wave excitation conditions on the output performance of OWC-TENG. g) Schematic diagram of the variation of the output current with respect to the time under 50 s excitation.

To further investigate the effect of water waves with different frequencies and amplitudes on the output performance of OWC-TENG, the results are shown in Figure 3c,e. The gap between the rotor and stator was controlled to be 1 mm and the wave height was adjusted to observe the extent to which the wave height affects the output performance of the device. The initial wave height was set at 0.1 m and the control frequency was 0.83 Hz. With the gradual increase of the wave height, the output voltage, current, and transferred charge of the OWC-TENG and the rotor speed gradually increase and reach the maximum values when the wave height is 0.25 m. The maximum output voltage, output current, transferred charge, and rotor speed are respectively 266.92 V, 23.65 μA, 141.42 nC, and 819 rpm. The first increase of the OWC-TENG outputs with the increase of wave height is due to the increase in the airflow speed generated by the OWC and the rotation speed of the air turbine TENG caused by the increased input wave energy. With further increasing the wave height, the output voltage, current, and transferred charge drop and keep almost stable. That may be due to the increase in the vortex effect of the waves, which may result in increased system damping and violent wave impacts, limiting the effective operation of the OWC and the TENG.

Subsequently, the influence of water wave frequency on the output performance of the OWC-TENG was investigated at a constant wave height of 0.25 m (Figure 3d,f). The initial frequency was set to be 0.33 Hz and the outputs reach the peak values as the wave frequency increases to 0.83 Hz. The transferred charge increases from 85.42 to 141.42 nC, and the output voltage increases from 167.90 to 266.92 V. The output current increases from 5.63 to 23.65 μA, and the rotor speed also increases from 360 to 819 rpm. However, as the frequency of the water wave continues to increase, the output performance of the OWC-TENG begins to decrease. This indicates that the improved structural parameters of the OWC-TENG are more suitable for collecting low-frequency and low-amplitude water wave energy, which meets the requirements of practical applications. It is possible that the

higher electrical outputs of the OWC-TENG under the 0.83 Hz and 0.25 m wave conditions are due to the fact that the vibration frequency under these conditions is close to or equal to the natural resonant frequency of the OWC-TENG system. At the resonating state, the vibration amplitude and energy outputs are maximized.

Therefore, under the optimal water wave conditions, the output voltage, current, and transferred charge are 266.92 V, 23.65 μA, and 141.42 nC, respectively, when the excitation is applied to the OWC-TENG device for about 50 s, as shown in Figure S5, Supporting Information. The inertial energy storage property of the OWC-TENG is well demonstrated in Figure 3g. Due to the inertia of the generator turbine of the OWC-TENG, its state of motion helps to store and release energy. When a wave lifts, the turbine receives the wave's impetus and begins to rotate, thus converting energy into inertial energy and storing it. When the wave recedes, the turbine continues to rotate, releasing the previously stored inertial energy. This inertial energy storage mechanism provides the OWC-TENG with stable energy conversion and output. At Stage 1, the rotor speed of the air turbine is gradually increased by the continuous excitation of the water waves, while the output current of the OWC-TENG gradually increases with the rotor speed, reaching the peak value at about 18 s and maintained at about 20 μA. Afterward, as shown in Stage 2, the efficiency of energy transfer varies as the phase difference between the wave and the OWC changes, but the output of the OWC-TENG has a small variation due to the presence of inertial energy storage in the OWC-TENG. So after 18 s, the output current varies in the range of 18–20 μA. The efficiency of the energy conversion reaches its maximum and the output reaches its maximum when the phase of the OWC-TENG is aligned with the phase of the waves in Stage 3, where the current is around 24 μA. Finally, in Stage 4, the TENG is working under the excitation of the tiny wave. In wave energy conversion systems, the input of wave energy is usually unstable, so energy caching is very important, and this result proves the usefulness of OWC-TENG for energy caching, which makes it better adapted to the collection of water wave energy at low frequencies.

To achieve large-scale water wave energy harvesting, arrays consisting of multiple generators are required, and TENG arrays can achieve high energy conversion efficiencies. **Figure** 4a,b shows photographs of the TENG and vector plots of wind speed variations obtained from simulations in the enclosure (see Figure S6, Supporting Information, for simulated trajectories and wind speed clouds). At the inlet, the velocity of the fluid is usually higher, followed by the rotor region, which is the core of the turbine. Here, the direction and acceleration of the fluid change, increasing the fluid velocity. As shown in Figure 4c and Figure S7, Supporting Information, experiments were carried out under optimal excitation conditions and it was observed that the transferred charge of the upper and lower generators was about 140.32 nC and the difference in output current was about 5.33 μA. In addition, we conducted charging experiments on the upper and lower generator units in the device that were not processed by the management circuit (Figure S8, Supporting Information) and charged a 680 μF capacitor to about 4.2 V. The experiments verified that the charging process takes about 550 s. It was observed that the output and charging efficiencies of the upper and lower OWC-TENG units were very similar. This result indicates that the output performance of the bidirectional air turbine is not affected by the difference between the high and low wind speeds within it, demonstrating the potential of the OWC-TENG in a longitudinal array. The OWC-TENG utilizes a non-contact mode of operation, resulting in lower frictional resistance. After an uninterrupted triggering of 200 000 cycles at the gap of 1 mm, the output current of the TENG device exhibits a small attenuation of below 5.6% (Figure S9, Supporting Information). Furthermore, the material wear is not visible in the scanning electron microscope (SEM) images (Figure S10, Supporting Information), verifying the good device durability of the OWC-TENG for water wave energy harvesting.

Figure 4d shows the power management circuit of the OWC-TENG for marine applications, in which the upper and lower TENG units are separately rectified through a rectifier bridge followed by their parallel connection. The components of our management circuit include two rectifier bridges (DB107), a voltage regulator (2EZ100D5), an inline ceramic capacitor (10 nF, 2 kV), a diode (1N4007), an I-beam inductor (10 mH) and a silicon-controlled rectifier (EC103M1). With the two units connected in parallel, the stabilized voltage output of the rectified OWC-TENG is 373.23 V and the output current is 55.45 μA, as shown in Figure 4e. The output of the device is almost doubled, demonstrating its good integration capability. The charging speeds of the upper and lower subunits of the device were then further compared in parallel and in series (Figure 4f). charging the 680 μF capacitor to 4.8 V took about 153 s in series while charging in parallel took only 30 s to reach the same voltage level. Therefore, the charging performance of the OWC-TENG was tested under parallel conditions (Figure 4g), and it can be seen that the charging time corresponding to each capacitance value in charging the capacitor to 4.6 V is as follows: 8 s for a 100 μF capacitor, 22 s for a 220 μF capacitor, 28 s for a 470 μF capacitor, and 60 s for a 1 mF capacitor.

After that, the output power was investigated for one unit and two units, and the test results are shown in Figure 4h,i. The maximum peak power of the TENG is 3.64 mW, and the average power is 1.60 mW, at the matched impedance of 10 MΩ. The upper and lower TENG modules are parallelly integrated with a maximum peak power of 5.28 mW and an average power of 2.89 mW, where the matched resistance is 5 MΩ. It can be found that with the gradual increase in the number of OWC-TENG generating units, the peak and average power and the corresponding power densities tend to increase. This proves that the OWC-TENG has a better ability to collect water wave energy after integration.

2.3. Application of OWC-TENG

Based on the independence and stability advantages of OWC-TENG in blue energy harvesting, we expect to use it as a power source for offshore Internet of Things (IoT) mobile nodes and applications, as shown in **Figure** 5a. In addition, the device can be used as an offshore buoy warning light that can continuously emit light and keep 117 light-emitting diodes (LEDs) flashing in intervals (Figure 5d). Remarkably, the device exhibits excellent sensitivity even under low-amplitude excitation conditions of 1 Hz and 0.1 m. It was able to make the LED function properly under very weak wave excitation, suggesting that OWC-TENG can

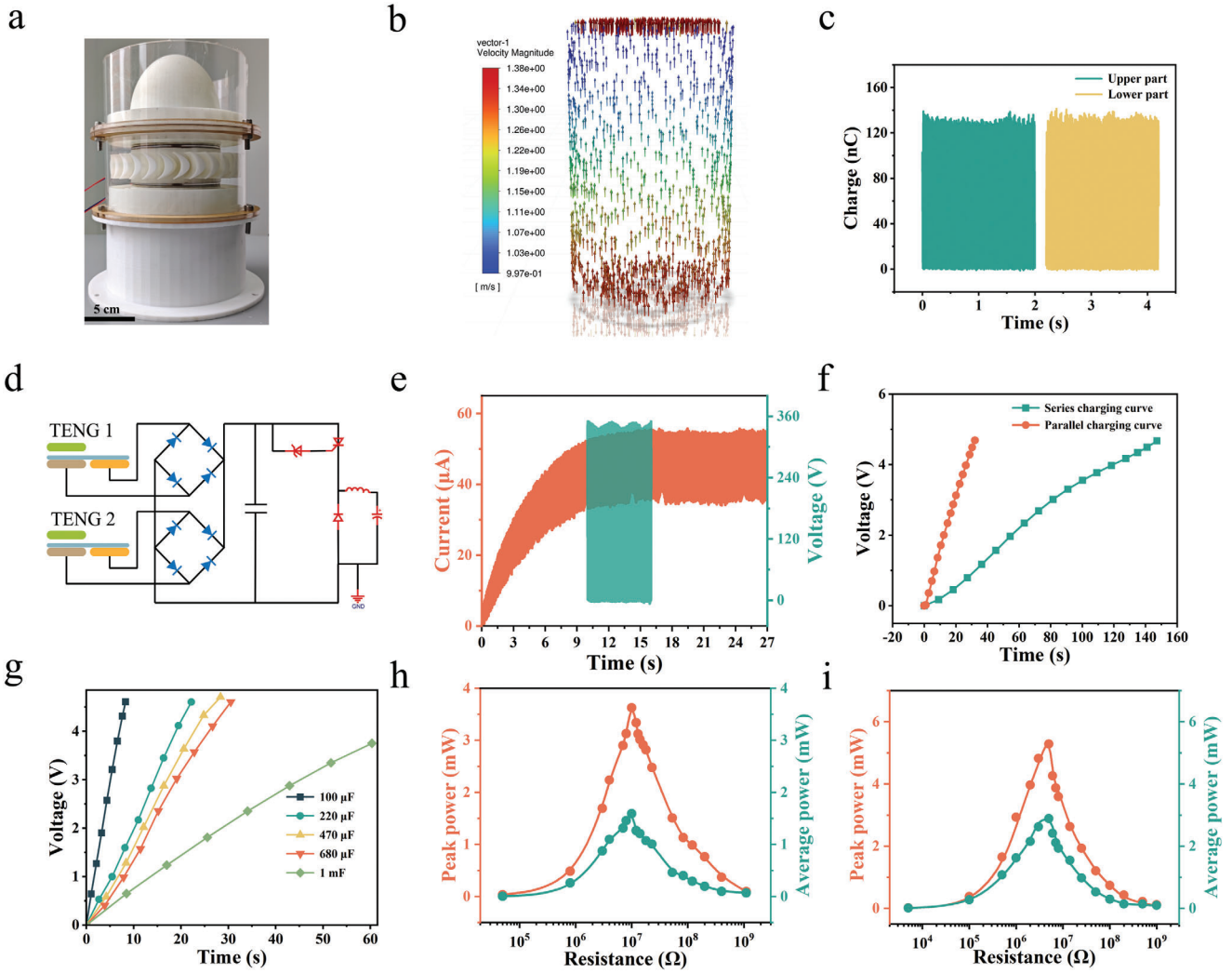

Figure 4. Electrical characteristics of OWC-TENG underwater wave triggering. a) Photograph of the air turbine TENG. b) Wind speed simulation of fan casing. c) Comparison of the charges transferred by the upper and lower generators. d) Power management circuit used in the OWC-TENG. e) Output current and output voltage of the rectified OWC-TENG. f) Charging diagram of upper and lower subunits in the OWC-TENG in series and parallel. g) Charging results of different capacitors under optimum excitation conditions. h) Peak and average powers of a subunit of OWC-TENG at different resistances. i) Peak and average power of two OWC-TENG integrated units at different resistances.

harvest energy from mild water waves (as shown in Video S2, Supporting Information). After confirming its excellent performance, it was further applied in wireless temperature sensing and offshore wind speed monitoring systems as a wave energy harvester toward self-powered systems for the IoTs. Wind speed is obtained by directly connecting a 2 mF storage capacitor (C_S) in parallel with the power generating unit and the anemometer, and by switching off the switch when the capacitor is charged to be above 5 V, as shown in Figure 5b,e (circuit shown in the inset) and Video S3, Supporting Information. For wireless temperature detection, as shown in Figure 5c,f (circuit in the inset) and Video S4, Supporting Information, when the capacitor is charged to be above 5 V, it can be automatically activated and continue to work without interruption within 3 s, and the temperature sensor sends temperature data to the computer software every 5 s for a duration of about 14 s. The results show that this TENG device can efficiently convert mechanical energy into electrical energy and has good responsiveness to different sources of strain and vibration. In addition, the device has a low cost and is easy to fabricate, making it potentially advantageous for practical applications. This makes TENG technology promising for renewable energy applications.

3. Conclusions

Inspired by conventional OWC devices for wave energy harvesting, a new system is demonstrated based on a new strategy for fluid absorption and utilization by a two-way air turbine for the first time. The system uses fluid oscillations to convert the irregular motion of waves into regular motion, extracts energy from low-frequency and low-amplitude waves, and uses an air turbine to convert mechanical energy into electrical energy. The device makes up for the shortcomings of OWC's electromagnetic generators in wave harvesting. Under the excitation conditions of a

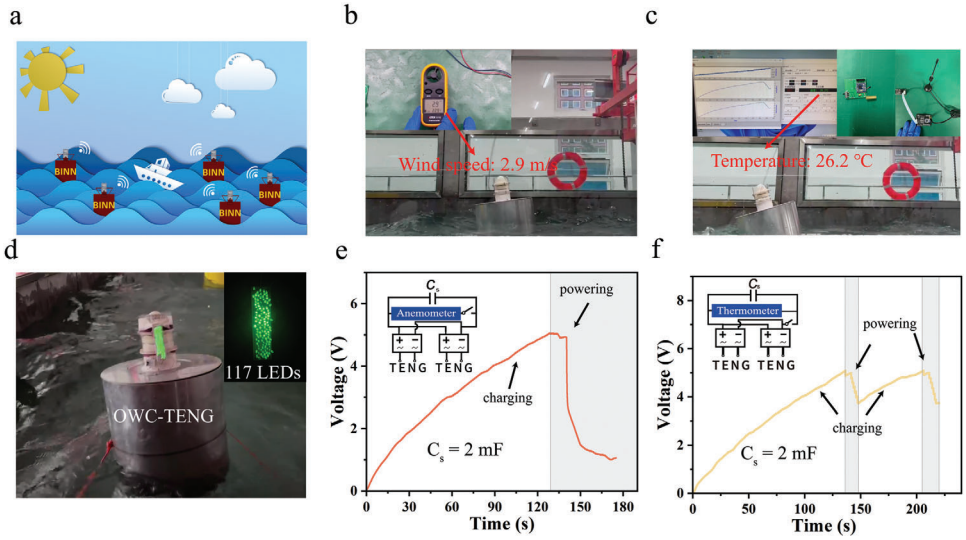

Figure 5. OWC-TENG powering electronic devices underwater wave triggering. a) Conceptual schematic of OWC-TENG. b) Photograph of powering the anemometer. c) Photograph of powering the wireless sensing thermometer. d) Photograph of lighting up the LEDs. e) Example of capacitor charging and discharging for powering the wireless thermometer. d) Photograph of lit LED. e) Example diagram of capacitor charging and discharging for powering the anemometer f) Example diagram of capacitor charging and discharging for powering the wireless thermometer.

frequency of 0.83 Hz and an amplitude of 0.25 m, the maximum peak power of the OWC-TENG power generation unit is 5.28 mW and the average power is 2.89 mW at a matched resistance of 5 MΩ, corresponding to an effective peak power density of 114.8 W m^{-3} and an effective average power density of 62.8 W m^{-3}. That can be used to construct self-powered ocean warning devices using ocean waves and provide a stable power supply for wireless temperature sensors and wind sensing systems. The results show that this TENG device is able to efficiently convert mechanical energy into electrical energy and is very responsive to different sources of strain and vibration. In addition, the device has low cost and is easy to fabricate, making it potentially advantageous for practical applications. Through further analysis and testing, the TENG device was also found to have high reliability and stability in terms of sustainable energy harvesting. Its self-powering nature allows it to require no external energy input, thus reducing the reliance on energy storage devices such as conventional batteries. This makes TENG technology a promising application in the field of renewable energy.

4. Experimental Section

Fabrication of the OWC-TENG Device: The OWC wave energy converter possessed the key components of float, water column chamber, and conduit. The float can partially or completely float on the water surface and move up and down with the waves. The float consisted of a main float body and a pendant swinging plate. The main float body was an aluminum alloy sleeve-like shell with a height of 0.6 m and a radius of 0.3 m. The shell consisted of a 0.003 m-thick inner wall, a 0.005 m-thick outer wall, and a closed hollow sandwich located between the inner and outer walls, which was used to provide buoyancy to keep the whole device floating on the water surface. The main float body had an internal cavity channel with a radius of 0.2 m in its center and a central through-hole with a radius of 0.1 m at the top of the channel for connection to the TENG section. The pendant oscillating plate had a thickness of 0.005 m and was fixed under the main float body by four connecting rods with a diameter of 0.01 m and a length of 1.01 m, and was arranged perpendicularly to the inner cavity channel. The water column chamber was located below the float, and as the waves pushed the float body up, the water level inside the water column chamber rose, squeezing the air inside the chamber through a conduit connected to the TENG.

The TENG device was mounted on the top of the inner cavity channel of the main float body with a two-way air turbine made by 3D printing technology, while the air turbine had two rows of fixed guide vanes symmetrically distributed on the stator on both sides of the rotor, and each row contained 26 guide vanes. The curvature line of the guide vanes consisted of straight lines and circular arcs, the number of rotor vanes on the rotor was 30, and the dynamic vane pattern line consisted of circular arcs on the pressure side and elliptical arcs on the suction side. Afterward, a super-lubricated ceramic bearing with an inner diameter of 6 mm and an outer diameter of 12 mm was embedded into the center hole of the stator, and an optical shaft with a diameter of 6 mm was embedded into the bearing so that the rotor can rotate smoothly under the triggering of external forces. The rotor and stator disc substrates of the power module were laser cut from epoxy glass fiber sheets with a thickness of 2 mm and a radius of 51 mm. The stator disc was made by PCB process, and the copper electrode layer with a thickness of 35 µm was fabricated on the substrate with an inner diameter of 12 mm and an outer diameter of 102 mm, and four equidistant rectangular grooves with a length of 32 mm and a width of 4 mm were cut on the stator disc, and four rabbit hairs trimmed to a length of 9 mm were placed in the grooves, and the rabbit hairs and stator discs were bonded by double-faced adhesive tape. A ring of 2 mm thickness was designed on the outermost edge of the stator's guide vanes, which was connected to the turbine housing, and a 9.3 mm long optical shaft connected the rotor to the stator. The polylactic acid substrate had an inner diameter of 151 mm, an outer diameter of 160 mm, and a thickness of 80 mm; and the acrylic cylindrical shell was divided into two layers with inner diameters of 154 mm, outer diameters of 160 mm, and thicknesses of 140 and 80 mm, respectively; the three were fixed by flange ring.

Electric Measurements of the OWC-TENG Device: The main instruments used in the experimental process were a Universal PLS6.75 laser cutting machine, a Keithley 6514 electrometer, and a wave tank. The laser cutter was mainly used to cut the shape of the acrylic plate, first of all, through the AutoCAD software to draw the pattern, import it into the laser cutter special software, and then process the specified shape. The electrometer was used to measure the output current, voltage, transferred

charges of the TENG, and the charging voltage on the capacitors. Various output signals and performance studies of the OWC-TENG were measured in the wave tank.

Supporting Information

Supporting Information is available from the Wiley Online Library or from the author.

Acknowledgements

S.Y., C.Z., Z.D., and Y.T. contributed equally to this work. The research was supported by the National Key R & D Project from the Minister of Science and Technology (2021YFA1201604, 2021YFA1201601), Industry-University Cooperation Project in Fujian Province University (2023H61010068), Fujian Provincial Natural Science Youth Funding (022J05155), Xiamen Science and Technology Bureau Nature Funding (3502Z20227057), Beijing Nova Program (20220484036), and Innovation Project of Ocean Science and Technology (22-3-3-hygg-18-hy).

Conflict of Interest

The authors declare no conflict of interest.

Data Availability Statement

The data that support the findings of this study are available from the corresponding author upon reasonable request.

Keywords

blue energy harvesting, high output power density, offshore Internet of Things, oscillating water column triboelectric nanogenerator, triboelectric nanogenerator

Received: December 5, 2023
Revised: February 2, 2024
Published online: February 16, 2024

[1] P. Cheng, Y. Liu, Z. Wen, H. Shao, A. Wei, X. Xie, C. Chen, Y. Yang, M. Peng, Q. Zhuo, X. Sun, *Nano Energy* **2018**, *54*, 156.
[2] W. Sheng, *Renewable Sustainable Energy Rev.* **2019**, *109*, 482.
[3] Y. Hu, H. Qiu, Q. Sun, Z. L. Wang, L. Xu, *Small Methods* **2023**, *7*, 2300582.
[4] Q. Shi, H. Wang, H. Wu, C. Lee, *Nano Energy* **2017**, *40*, 203.
[5] Y. Wang, Z. Qian, C. Zhao, Y. Wang, K. Jiang, J. Wang, Z. Meng, F. Li, C. Zhu, P. Chen, H. Wang, M. Xu, *Adv. Mater. Technol.* **2022**, *8*, 2201245.
[6] Z. L. Wang, *Mater. Today* **2017**, *20*, 74.
[7] Z. L. Wang, T. Jiang, L. Xu, *Nano Energy* **2017**, *39*, 9.
[8] Y. Luo, R. Tao, G. Peng, *Ocean Eng.* **2022**, *245*, 110429.
[9] Z. Liu, C. Xu, X. Zhang, D. Ning, *Renewable Sustainable Energy Rev.* **2023**, *184*, 1364.
[10] D. Gallutia, M. Tahmasbi Fard, M. Gutierrez Soto, J. He, *Ocean Eng.* **2022**, *252*, 111105.
[11] H. Wang, Q. Zhu, Z. Ding, Z. Li, H. Zheng, J. Fu, C. Diao, X. Zhang, J. Tian, Y. Zi, *Nano Energy* **2019**, *57*, 616.
[12] B. Zhao, Z. Li, X. Liao, L. Qiao, Y. Li, S. Dong, Z. Zhang, B. Zhang, *Nano Energy* **2021**, *89*, 106381.
[13] M. Yin, Y. Yu, Y. Wang, Z. Wang, X. Lu, T. Cheng, Z. L. Wang, *Extreme Mech. Lett.* **2019**, *33*, 100576.
[14] X. Chen, H. He, P. Sun, *J. Mar. Sci. Appl.* **2022**, *21*, 155.
[15] X. Cao, H. Zhou, Y. Zhou, Y. Hu, Y. Wang, Z. L. Wang, Q. Sun, *Adv. Mater. Technol.* **2023**, *8*, 2300327.
[16] O. R. Chowdhury, H.-g. Kim, D.-g. Park, Y. Cho, C. Shin, J. Park, *Int. J. Smart Home* **2015**, *9*, 197.
[17] W. Li, K. T. Chau, J. Z. Jiang, *IEEE Trans. Magn.* **2011**, *47*, 2624.
[18] S. Tian, X. Wei, L. Lai, B. Li, Z. Wu, Y. Dai, *Nano Energy* **2022**, *102*, 107669.
[19] I. Goncalves, C. Rodrigues, J. Ventura, *Adv. Energy Mater.* **2024**, *14*, 2302627.
[20] Z. Lin, B. Zhang, H. Zou, Z. Wu, H. Guo, Y. Zhang, J. Yang, Z. L. Wang, *Nano Energy* **2020**, *68*, 104378.
[21] Y. Xi, H. Guo, Y. Zi, X. Li, J. Wang, J. Deng, S. Li, C. Hu, X. Cao, Z. L. Wang, *Adv. Energy Mater.* **2017**, *7*, 1602397.
[22] G. Zhu, J. Chen, T. Zhang, Q. Jing, Z. L. Wang, *Nat. Commun.* **2014**, *5*, 3426.
[23] Z. Xu, L. Chen, Z. Zhang, J. Han, P. Chen, Z. Hong, T. Jiang, Z. L. Wang, *Small* **2023**, https://doi.org/10.1002/smll.202307288.
[24] P. Chen, J. An, S. Shu, R. Cheng, J. Nie, T. Jiang, Z. L. Wang, *Adv. Energy Mater.* **2021**, *11*, 2003066.
[25] G. Liu, H. Guo, S. Xu, C. Hu, Z. L. Wang, *Adv. Energy Mater.* **2019**, *9*, 1900801.
[26] L. Liu, Q. Shi, C. Lee, *Nano Energy* **2020**, *76*, 105052.
[27] A. F. O. Falcão, L. M. C. Gato, E. P. A. S. Nunes, *Renewable Energy* **2013**, *50*, 289.
[28] T. Setoguchi, M. Takao, *Energy Convers. Manage.* **2006**, *47*, 2382.
[29] W. Gao, *ANSYS AQWA Software Introduction and Improvement*, China Water & Power Press, Beijing, China **2018**.